The Ternary System Au–Cu–Sn

O. B. Karlsen, A. Kjekshus* and E. Røst

Department of Chemistry, University of Oslo, Blindern, N-0315 Oslo 3, Norway

Karlsen, O. B., Kjekshus, A. and Røst, E., 1992. The Ternary System Au–Cu–Sn. – Acta Chem. Scand. 46: 147–156.

The phase relations in the Au–Cu–Sn system have been examined by powder X-ray diffraction, metallography, scanning electron microscopy and thermal analysis. The range of homogeneity of the various phases, tie-lines and tie-triangles is shown in an isothermal (horizontal) section of the phase diagram at 360 °C. Au and Cu can to a large extent be mutually exchanged in all phases. A continuous range of homogeneity is found between AuSn (δ) and Cu_6Sn_5 (η) with a maximum variation of ~3.5 atom % Sn at equal amounts of Au and Cu. The three genuine ternary phases, labelled A, B and C, have, respectively, the homogeneity ranges $Au_{42}Cu_{38}Sn_{20}$–$Au_{47}Cu_{33}Sn_{20}$, $Au_{11}Cu_{69}Sn_{20}$–$Au_{38}Cu_{42}Sn_{20}$ (with a maximum broadening of ~2.5 atom % Sn) and $Au_{330}Cu_{337}Sn_{333}$–$Au_{370}Cu_{297}Sn_{333}$ at 360 °C. The difference between Au and Cu atomic volumes show a systematic increase with increasing Sn content, and this is qualitatively interpreted as evidence for transfer of electron density from Sn to Au. Alloys with 20 atom % Sn are examined at different temperatures, and a vertical (pseudo-isoplethal) section through the phase diagram is presented for this Sn content. A number of isothermal cross-sections are advanced for the Au-rich part of the phase diagram. Attention is paid to the phase equilibrium in an invariant four-phase region.

This report concerning the system Au–Cu–Sn is a continuation of a short communication[1] on the three genuine ternary phases in the system. Like other tin systems, Au–Cu–Sn has provided a number of challenging characterization problems – for metallography and X-ray diffraction in particular.

As a background, it is convenient to start with a brief survey of the binary systems Au–Cu, Au–Sn and Cu–Sn. The former is the least interesting in this connection because already small amounts of added tin seem to shift the ordering temperatures for the various Au–Cu superstructures below the present low-temperature limit of 360 °C. Au and Cu form a continuous solid solution (with an f.c.c.-type structure) above ~410 °C, while at lower temperatures superstructures are formed about Au_3Cu, AuCu and $AuCu_3$.[2] Sato and Toth[3] have shown that 8 atom % Sn has lowered the ordering temperature of AuCu enough to prevent the ordered phase from being formed.

The phase relationships in the Au–Sn system are shown in Fig. 1. The situation at 360 °C is of particular interest for the present work. The ζ-phase (10–17 atom % Sn)[4] takes an h.c.p.-type structure, whereas the β-phase ($Au_{10}Sn$; 9.1 atom % Sn)[5] takes a superstructure of the former with a doubled *c*-axis (somewhat shorter than 2*c* for ζ). The formation temperatures for the β- and ζ-phases have been subject to discussion. According to Okamoto and Massalski[6] the ζ-phase forms peritectically at ~500 °C and the β-phase peritectoidally at a somewhat lower temperature. Legendre *et al.*[7] report that both phases form peritectically at 532 and 523 °C for β and ζ, respectively, but in a later compilation[8] the peritectic temperature for the ζ-phase is somewhat lower, 519 °C. In accordance with the present work, the results of Ref. 7 are accepted in Fig. 1. The δ-phase (AuSn, 50–50.5 atom % Sn) takes the NiAs-type structure, and melts congruently at 419 °C. The ε-phase ($AuSn_2$; $AuSn_2$-type structure) and η-phase ($AuSn_4$; $PtSn_4$-type structure) have both melted at 360 °C.

The phase diagram for Cu–Sn is given in Fig. 2. This is the currently accepted phase diagram from Hansen and Anderko[9] with the exception that the lower-temperature limit of the phase δ has been increased so that it accords with the present work. Cu dissolves some 6 atom % Sn around 360 °C. The δ-phase ($Cu_{41}Sn_{11}$) has a cubic γ-brass-like structure which is a superstructure based on 8 b.c.c. γ-brass-type cells.[10,11] The ε-phase (Cu_3Sn, 23.5–25 atom % Sn) takes an orthorhombic structure which is described as a long-periodic superstructure of a Cu_3Ti-like basis (tenfold *b*-axis).[12] The eutectoid transition temperature of the δ-phase has been considered by many authors (cf. Ref. 9), and the results vary from 325 to 380 °C. The η-phase with an NiAs-type structure has a narrow range of homogeneity around Cu_6Sn_5.

The present authors[1] have already briefly reported on three genuine ternary phases, labelled A, B and C, in the Au–Cu–Sn system. A and B are found at, or around, 20 atom % Sn and C at 33.3 atom % Sn. The phases B and C have also peripherally been mentioned before in the literature.[13] Phase A takes a cubic γ-brass-type structure (with 52 atoms per unit cell), and we reported a range of homogeneity between $Au_{43}Cu_{37}Sn_{20}$ and $Au_{49}Cu_{31}Sn_{20}$ at 360 °C. Phase B has a cubic β-Mn-like structure (with 20 atoms per

* To whom correspondence should be addressed.

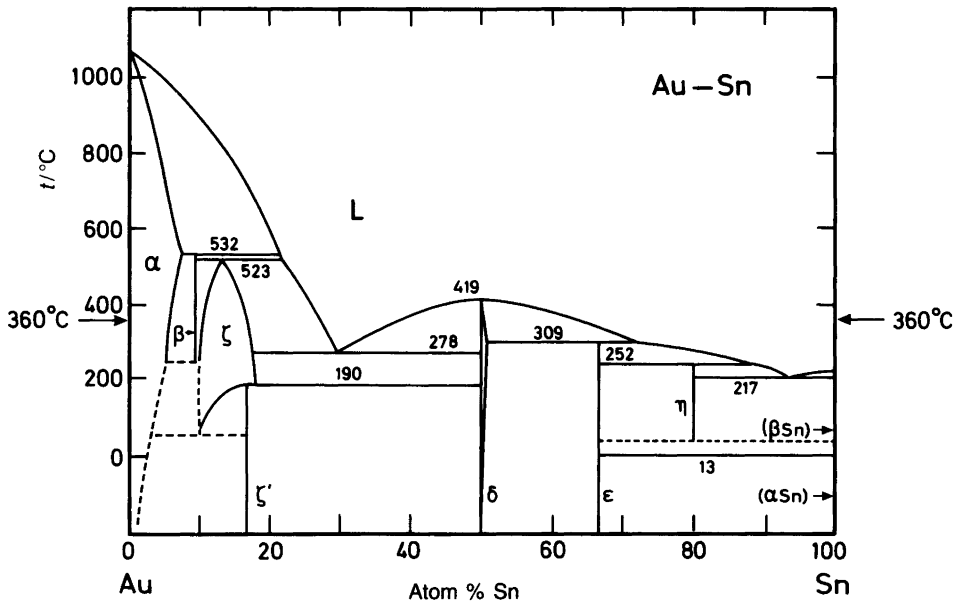

Fig. 1. Binary phase diagram for the system Au–Sn. High-temperature limits for phases β and ζ are from Ref. 7; the rest of the diagram is based on the compilation in Ref. 6.

unit cell), and we found a range of homogeneity at 360 °C from $Au_{12}Cu_{68}Sn_{20}$ to $Au_{36}Cu_{44}Sn_{20}$, with some broadening with respect to the Sn content also. Phase C has a tetragonal La_2Sb-like structure (with 12 atoms per unit cell) and a maximum extension at 360 °C from $Au_{330}Cu_{337}Sn_{333}$ to $Au_{370}Cu_{297}Sn_{333}$ and a virtually fixed content of 33.3 atom % Sn.

Experimental

Samples were made by melting (heating at 1100–1200 °C for ~1 min under vigorous shaking) appropriate amounts of 99.95 % Au (K. A. Rasmussen), 99.9 % Cu (J. T. Baker) and 99.98 % Sn (E. Merch) in sealed, evacuated silica-glass tubes. This initial heat treatment was in most cases concluded by quenching the samples from the molten state into ice water. Selected samples were also cooled slowly from the molten state to room temperature. Most of the samples were afterwards annealed at 360 °C (for 1–2 days) or another desired temperature (controlled within ±5 °C) and then quenched into ice water.

Specimens for X-ray powder diffraction (XPD) were obtained by crushing a part of a given sample to a fine powder and then repeating the final heat treatment on this selection. The ductile samples (viz. samples rich in the phases α, β or ζ) were powdered by filing, but otherwise treated as the rest of the samples. All samples were checked for homogeneity and characterized by XPD using Guinier Hägg cameras with Cu $K\alpha_1$ radiation and Si as internal standard. High-temperature XPD patterns were obtained

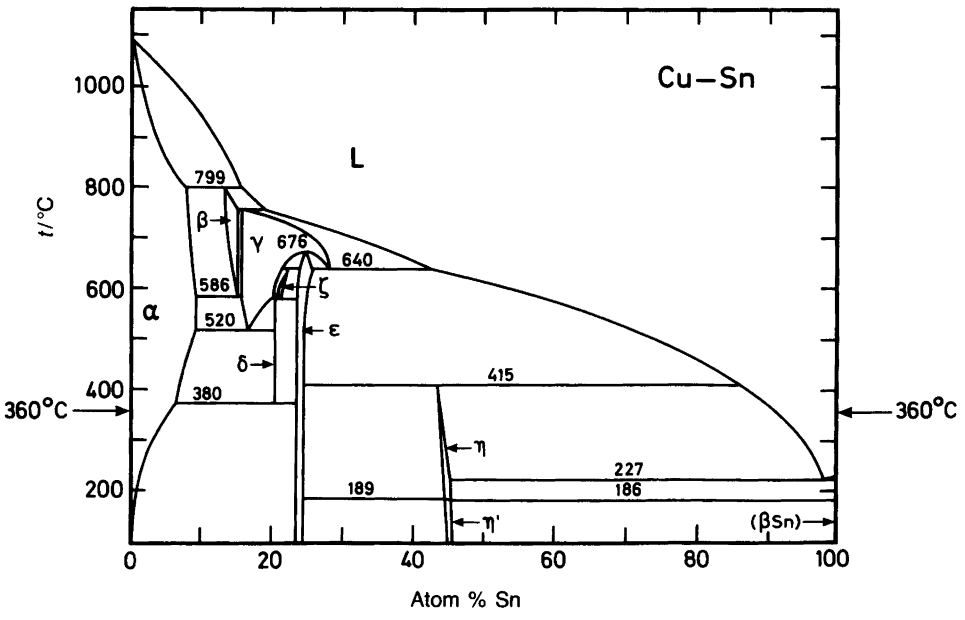

Fig. 2. Binary phase diagram for the system Cu–Sn. The low-temperature limit for phase δ is from the present work; the rest of the diagram is based on the compilation in Ref. 9.

at temperatures between 20 °C and, depending on the composition, 400–900 °C using a Guinier Simon camera (Enraf–Nonius) and Cu $K\alpha_1$ radiation. The samples were placed in closed silica-glass capillaries and heated at a rate of 20–40 °C h^{-1}. Position and intensity measurements of the reflections were carried out using a Nicolet L18 film scanner controlled by the SCANPI program system.[14] Unit-cell parameters were obtained using the CELLKANT program.[15]

Differential scanning calorimetry (DSC) measurements were made between 20 and 600 °C with a Mettler TA 3000 thermoanalyzer system, using 50–150 mg specimens (treated as for XPD, but slowly cooled to room temperature over a period of one week) contained in sealed glass holders. Heating or cooling rate was usually 5 °C min^{-1}. Differential thermal analysis (DTA) above 600 °C was performed by a Netzsch (404 EP) instrument, the results obtained from 20 to 600 °C being fully compatible with those acquired by DSC.

Metallographic cross-sections were usually examined for 2 or 3 specimens from different parts of the sample. Specimens with the melting point below ~400 °C were cold-mounted in Specifix (Struers), whereas resin (Struers, No. 3) was used otherwise. Grinding was made with silicon carbide paper under water cooling, and polishing was performed according to the Struers DP procedure. A thin layer of carbon was evaporated on to specimens for electron microscopy, and specimens for optical microscopy were mostly etched with a mixture of $FeCl_3$ and HCl in either ethanol or water. Optical microscopy was carried out with a Reichert Zetopan-Pol microscope, and scanning electron microscopy (SEM) with a JEOL (JSM-35; PTG-1000 energy-dispersive X-ray analyzer) instrument.

Isothermal (horizontal) section at 360 °C

A major part of the present study is focussed on the phase situation at 360 °C. Fig. 3 gives the location of the most relevant samples in the Au–Cu–Sn triangle, and different symbols are used to mark whether these are established as one-, two- or three-phase at 360 °C. The experimentally determined (by metallography, SEM-analysis and/or comparison of unit-cell dimensions) ranges of homogeneity together with tie-lines and tie-triangles at 360 °C are also shown in the figure. The designations for the binary phases comply with the usual notations, except for the phase which extends from AuSn (δ) to Cu_6Sn_5 (η) and is referred to as δ/η in this paper. The genuine ternary phases of the Au–Cu–Sn system are designated A, B and C.

The α-phase. Both Au and Cu dissolve some 6–7 atom % Sn at 360 °C (Figs. 1 and 2), and the present study suggests that the solid solubility is of the same magnitude for Au–Cu alloys. No sign of any ordering of the random f.c.c.-type structure of the α-phase was found for samples rich in Sn and annealed at 360 °C. This is in agreement with the findings of Sato and Toth.[3] The stability ranges of the ordered structure of the α-phase have not been investigated further, and their occurrence is neglected in Fig. 3 and the succeeding illustrations.

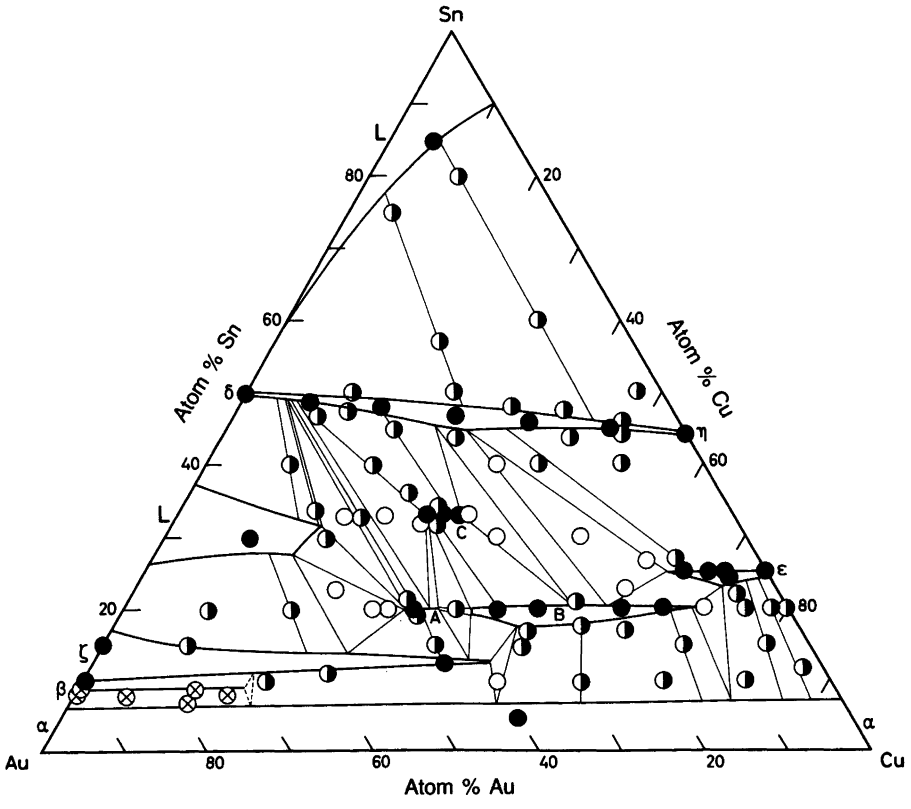

Fig. 3. Location of selected (relevant) samples in the Au–Cu–Sn triangle. Filled, half-filled and open circles represent samples containing one, two and three phases, respectively, after annealing at 360 °C. Au-rich samples which had not attained complete equilibrium are marked by open circles with a cross. Phase limits, tie-lines and tie-triangles determined by direct experiments are marked by solid lines.

The β- and ζ-phases. The existence of the β-phase is confirmed, but in accordance with the findings of Schubert *et al.*[5] it proved impossible to prepare phase-pure samples of β (even after 30 days annealing at 360 °C of massive samples as well as filings). The Sn content of β appears to be fixed at ~9 atom % Sn in the binary Au–Sn system, since the unit-cell parameters [a = 290.1(4), c = 952.4(6) pm] are the same regardless of whether β is mixed with α or ζ. This condition on the composition of β is probably also maintained in the ternary region. The gold-rich boundary of the ζ-phase is close to 10 atom % Sn, with a = 290.2(3) and c = 477.9(4) pm. These results are in reasonable agreement with Refs. 4 and 5.

Au can be replaced by appreciable amounts of Cu in both phases. At 360 °C the β-phase can accommodate ~20 atom % Cu. The unit-cell dimensions decrease smoothly with increasing degree of Cu for Au substitution, and for 18 atom % Cu, near the phase limit, a = 285.9(3) and c = 939.3(6) pm are obtained. In the ζ-phase more than half of Au can be substituted by Cu. At 360 °C the phase limit is close to 40 atom % Au ($Au_{40}Cu_{47}Sn_{13}$). The unit-cell dimensions decrease smoothly for ζ also: a = 277.3(3) and c = 453.9(5) pm for the phase boundary at 360 °C.

The α-, β- and ζ-phases are all ductile and can thus not be crushed.

The δ-phase. The δ-phase ($Cu_{41}Sn_{11}$) was obtained as phase-pure after heat treatment at 550 °C and subsequent quenching [a = 1796.4(8) pm, as compared with 1796.5 pm according to Ref. 10]. After careful crushing, this sample was divided in different portions, which were annealed at various temperatures for one week and then quenched. The results show that annealing temperatures at and above 380 °C retain the δ-phase, whereas annealings at and below 370 °C result in partial conversion to α and ε. This stipulates the eutectoid transition temperature of δ to between 370 and 380 °C (see Introduction). The δ-phase is, moreover, not observed in the ternary samples annealed at 360 °C, and accordingly δ does not enter Fig. 3.

The ε-phase. The substitution of Au for Cu in the ε-phase gives rise to an increase in the unit-cell dimensions, the variation in the sub-cell dimensions for $Au_xCu_{75-x}Sn_{25}$ being shown in Fig. 4. As seen from the figure, the maximum solubility amounts to ~12 atom % Au at 360 °C. The amount of tin can be varied between some 23 and 25 atom % Sn, and the unit-cell dimensions also increase with increasing Sn content. The Sn-poorest samples in the ternary field appear to take a somewhat different superstructure, as evidenced by changes in the weak XPD superstructure reflections. A further examination of this feature is, however, not undertaken.

The δ/η-phase. There exists a complete solid solubility between AuSn and Cu_6Sn_5 at 360 °C, and this δ/η-phase takes a regular to partly filled NiAs-type structure, with random distributions of the Au and Cu atoms over the relevant

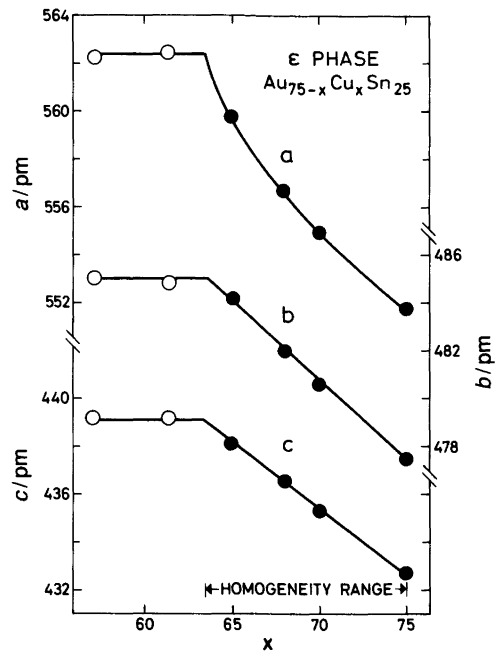

Fig. 4. Unit-cell dimensions plotted versus x in $Au_{75-x}Cu_xSn_{25}$ for the orthorhombic sub-cell of the ε-phase (samples annealed at 360 °C). Filled and open circles refer to one- and three-phase samples, respectively. Estimated error limits do not exceed the size of the symbols.

sublattice(s). As seen from Fig. 3, the homogeneity range of δ/η widens appreciably with respect to the Sn content for intermediate $n_{Cu}/(n_{Cu} + n_{Au})$ mole fractions. At, say, the equiatomic Cu/Au ratio the homogeneity range extends from ~45 to 48.5 atom % Sn at 360 °C, corresponding to unit-cell dimension variations between a = 430.2(4), c = 532.9(5) pm and a = 425.4(4), c = 527.9(6) pm, respectively. The unit-cell volume thus increases with decreasing Sn content, which is fully consistent with the condition that the excess of Au and Cu fill up bipyramidal holes in the Sn-poor field.

Fig. 5 shows that the unit-cell dimensions decrease monotonically when $n_{Cu}/(n_{Cu} + n_{Au})$ increases, the Sn content (in atom %) of the samples varying as $50 - 6n_{Cu}/(n_{Cu} + n_{Au})$ in order to keep within the homogeneity range of the δ/η-phase (cf. Fig. 3). It may be significant to note that c changes linearly with $n_{Cu}/(n_{Cu} + n_{Au})$, whereas a shows a kink at ~0.75. The latter behaviour is apparently not correlated with other properties of the δ/η-phase covered by the present study.

In accordance with the results summarized in Figs. 1 and 2, there is only a slight variation in the Sn content at the binary ends of the δ/η-phase at 360 °C. The present findings fully comply with those of Jan *et al.*[16] for δ (unit-cell variation between a = 432.2, c = 552.3 pm and a = 431.4, c = 551.7 pm over the range 50.0–50.5 atom % Sn). The homogeneity range of η is centred around 44 atom % Sn at 360 °C and has about the same width as δ [unit-cell dimensions being established as a = 421.9(5), c = 510.8(6) pm

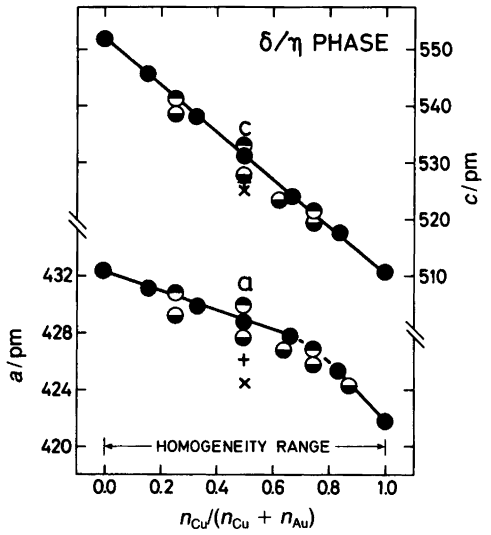

Fig. 5. Unit-cell dimensions as a function of $n_{Cu}/(n_{Cu} + n_{Au})$ mole fraction for the δ/η-phase (samples annealed at 360 °C). Estimated error limits do not exceed the size of the symbols. Points marked ● refer to one-phase samples with Sn content (in atom %) defined by $50 - 6n_{Cu}/(n_{Cu} + n_{Au})$, ◓ to the Sn-poor phase limit, ◒ to the Sn-rich phase limit. Samples of $Au_{25}Cu_{25}Sn_{50}$ annealed at 300 and 250 °C are marked as + and ×, respectively.

and a = 421.5(4), c = 510.3(4) pm for two-phase samples with 43 (η + ε) and 47 (η + L) atom % Sn, respectively]. When the annealing temperature is lowered the phase boundaries of η are shifted towards higher Sn content, as is nicely demonstrated by the fact that the ε-phase separates out when $Cu_{56}Sn_{44}$ is cooled slowly from 360 °C. This feature is probably the main reason for the poor match between the present unit-cell dimensions (*vide supra*) and the old findings of Westgren and Phragmén.[17]

Samples of δ/η with different $n_{Cu}/(n_{Cu} + n_{Au})$ mole fractions have also been quenched after annealing below 360 °C, and unit-cell dimensions for samples with $n_{Cu}/(n_{Cu} + n_{Au})$ = 0.50 are included in Fig. 5 to illustrate the broadening of the homogeneity range. A sample of, say, $Au_{25}Cu_{25}Sn_{50}$, which at 360 °C consists of δ/η plus 4–5 % melt phase, has reduced the content of melt phase considerably at 300 °C and has become one-phase δ/η at 250 °C [a = 424.4(5), c = 525.4(6) pm]. An adjacent composition $Au_{265}Cu_{265}Sn_{470}$, which is one-phase at 360 °C, disengages phase B when it is subjected to lower annealing temperatures. In general terms this shows that the Sn content of ternary δ/η is increased when the annealing temperature is lowered.

The melt phases. Two separate melt phases occur in the Au–Cu–Sn phase diagram at 360 °C (Fig. 3). One extends from the eutectic point at ~29 atom % Sn in the Au–Sn system and the other encompasses the Sn-rich corner of Fig. 3. The extensions of the melt phases were determined by metallography and SEM analyses. If a sample which is in a partially molten state at 360 °C is quenched, the melt solidifies into a fine-grained matrix, which is easily detectable by optical microscopy. The composition of the matrix represents the composition of the melt, and can be determined by SEM analysis.

The A-phase. Identificational documentation for the A phase is given in Ref. 1. Re-evaluation of the data shows that the extension of its homogeneity range at 360 °C goes from $Au_{42}Cu_{38}Sn_{20}$ to $Au_{47}Cu_{33}Sn_{20}$ (viz. 42–47 atom % Au rather than 43–49 atom % Au reported in Ref. 1). Any extension of the homogeneity range with respect to the Sn component is limited to a narrow field around 20 atom % Sn, since samples with 19.5 and 20.5 atom % Sn contain the phases ζ and δ/η, respectively. The temperature variation of the homogeneity range and other aspects of the A-phase are considered below, and the structure determination will be reported separately.

The A-phase, which takes a γ-brass-type structure, shows a structural relationship with the δ-phase ($Cu_{41}Sn_{11}$), which also crystallizes with a γ-brass-like structure, but with a doubled cubic lattice parameter. When the composition variation of the a-axis for A ($Au_{80-x}Cu_xSn_{20}$) in Fig. 6 is extrapolated to x = 80, i.e. 0 atom % Au, a cell dimension of nearly half of that for the δ-phase is obtained. The δ-phase is, moreover, found in samples with nominal composition $Au_5Cu_{75}Sn_{20}$ quenched from 550 °C, and also $a/2$ of these fits the extrapolation in Fig. 6. However, it should be stressed that there is no continuous conversion between the phases A and δ.

A metastable phase, with composition 20.5 ± 1.5 atom % Sn, γ-brass-type structure and a = 980 pm has also been reported in the Au–Sn system.[18] However, the preparation of this phase requires use of the splat cooling technique (very rapid quenching of melt against a cooled copper

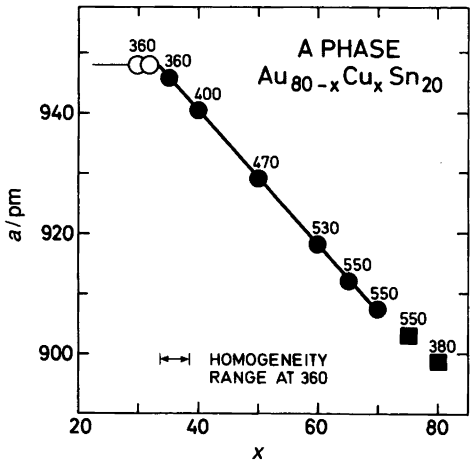

Fig. 6. Unit-cell dimensions plotted versus x in $Au_{80-x}Cu_xSn_{20}$ for phase A. Filled and open circles represent one- and three-phase samples, respectively. Squares correspond to $a/2$ for the δ-phase. Estimated error limits do not exceed the size of the symbols. Annealing temperatures (in °C) are given above each symbol. Note the narrow homogeneity range at 360 °C.

block), and it is assumed to be thermodynamically unstable even at low temperatures.[19] When the lattice parameter for phase A is extrapolated to $Au_{80}Sn_{20}$ a value of 985 pm is obtained. This suggests that the homogeneity range of A may extend to the binary end $Au_{80}Sn_{20}$, although portions of it may be metastable.

The B-phase. Identificational documentation for the B-phase is found in Ref. 1. At 360 °C the homogeneity range of B (which have the character of a low-temperature phase relative to A) extends from $Au_{11}Cu_{69}Sn_{20}$ to $Au_{38}Cu_{42}Sn_{20}$. This range is somewhat extended compared with our earlier report.[1] The limits for the variation in the Sn content are, however, maintained as 18 to 20.5 atom % Sn. At 300 °C the homogeneity range extends to 35 atom % Cu, and the Cu-poor phase limit reaches probably an even lower value below 300 °C.

As seen from Fig. 7 the relationship between the cubic lattice parameter and the composition variable x of $Au_{80-x}Cu_xSn_{20}$ consists of two linear sections which intersect at $x = 55$.

The fact that phase B is formed at low temperature through a solid-state reaction makes it difficult to obtain equilibrium. This is particularly problematic on the Au-rich side of phase B, where long annealing periods (at the low temperature concerned; *vide supra*) are needed to get rid of the last traces of phase A. On the Cu-rich side, the homogeneity range terminates in a three-phase field with α, ε and B (Fig. 8), all formed below 550 °C. Owing to these experimental difficulties, a systematic determination of the phase limits of B was not attempted.

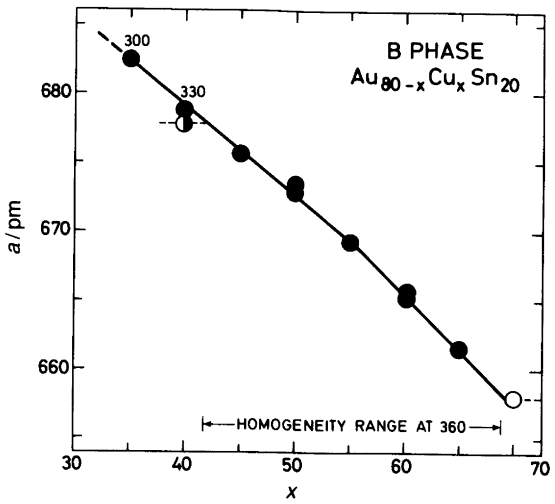

Fig. 7. Unit-cell dimension plotted versus x in $Au_{80-x}Cu_xSn_{20}$ for phase B. Filled, half-filled and open circles represent one-, two- and three-phase samples, respectively. Annealing temperatures (in °C) are given when different from 360 °C. Estimated error limits do not exceed the size of the symbols.

The narrow range of homogeneity with respect to the Sn content may be illustrated by the results for $Au_{26}Cu_{56}Sn_{18}$ [a = 667.8(5) pm for B, plus traces of α] and $Au_{25}Cu_{54}Sn_{21}$ [a = 669.4(5) for B, plus small amounts of δ/η]. The unit

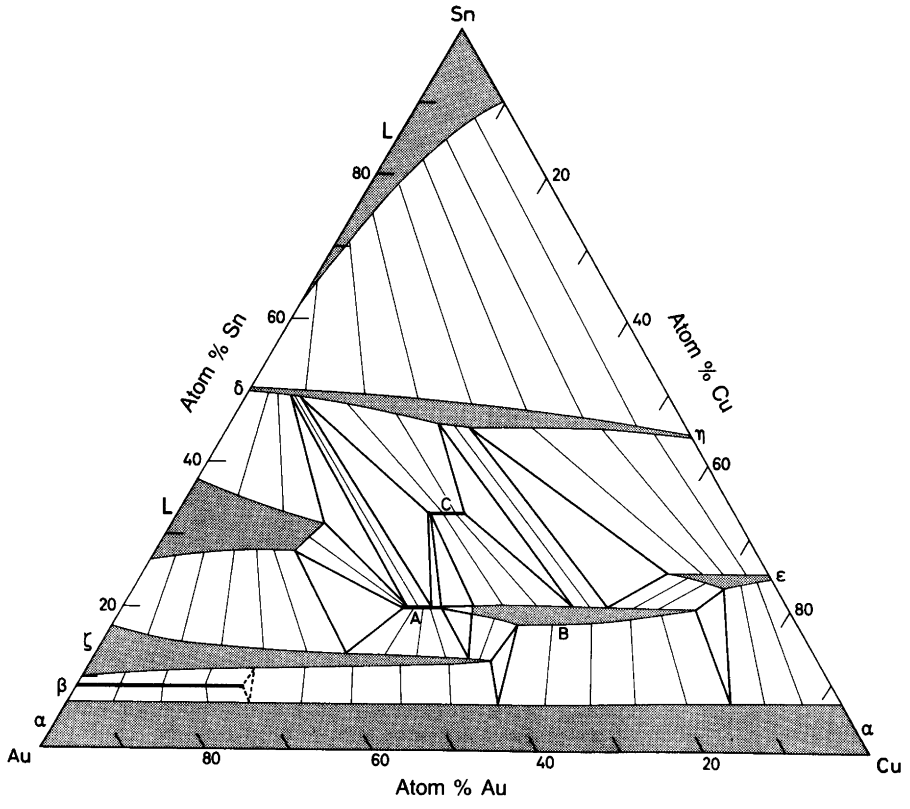

Fig. 8. Isothermal cross-section of the Au–Cu–Sn phase diagram at (or near) 360 °C. One-phase regions appear as shaded areas or thick lines, two-phase regions are shown by tie-lines and three-phase fields are exhibited by open tie-triangles. Superstructure orderings of α are neglected (see text).

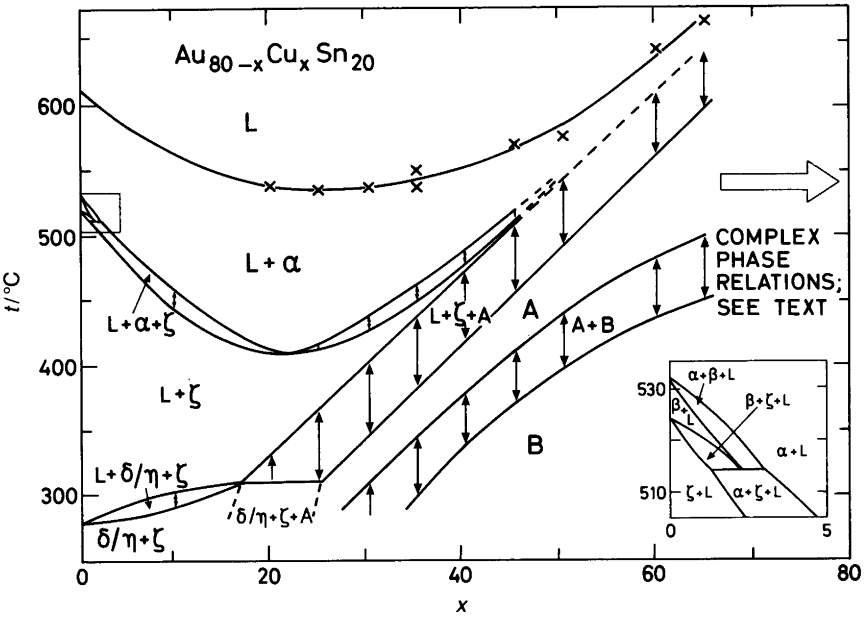

Fig. 9. Phase relationships at different temperatures for $Au_{80-x}Cu_xSn_{20}$ (20 atom % Sn fixed). Double arrows represent width of TA peaks and crosses liquidus temperatures (see Fig. 10 and text). Inset gives a principle sketch of phase relationships for α, β, ζ and L.

cell volume of B thus increases with increasing Sn content (as opposed to δ/η, see Fig. 5).

The structure determination of phase B will be accounted for in a separate paper.

The C-phase. The metallographic examination shows unequivocally that phase C is formed through a solid-state reaction, for say the $Au_{347}Cu_{320}Sn_{333}$ sample from δ/η and B at ~370 °C. Samples of $Au_{347}Cu_{320}Sn_{333}$, which were quenched from above 370 °C and then annealed for a few hours at 360 °C, show that phase C has been formed along the boundaries between δ/η and B. After about 30–40 h annealing at 360 °C such samples were converted into phase-pure C. In more Au-rich samples, phase A will also be represented in the matrix from which C is formed. The formation temperature for phase C does apparently not change appreciably with the Au to Cu atom ratio.

Documentation data for identification of phase C are reported in Ref. 1, and the structure determination will be communicated separately.

As reported in Ref. 1, phase C has a virtually fixed content of 33.3 % Sn and also a narrow homogeneity range with respect to Au and Cu at 360 °C. The tetragonal unit-cell dimensions increase approximately linearly between a = 407.3(2) and c = 1292.1(6) pm for the Au-poor phase limit of 33 atom % Au and a = 408.8(3) and c = 1300.7(6) pm for the Au-rich limit at 37 atom % Au.

The results considered so far are used to construct the isothermal cross-section of the complete Au–Cu–Sn phase diagram at 360 °C in Fig. 8, including ranges of homogeneity for all phases and tie-lines and tie-triangles.

Vertical (pseudo-isoplethal) section at 20 atom % Sn

Owing to the limited time and resources available for this study, it was decided to concentrate the attention of the influence on temperature variation mainly to a section of the Au–Cu–Sn phase diagram at 20 atom % Sn, where two of the new, interesting phases occur. The results summarized in Fig. 9 are based on thermal analysis (TA), XPD examination of quenched samples and high-temperature XPD work. The most Cu-rich part of Fig. 9 is not depicted, since the situation here is so unclear that much more exhaustive investigations are required before reasonably safe conclusions can be drawn.

The TA data for the $Au_{45}Cu_{35}Sn_{20}$ sample in Fig. 10 may serve to illustrate how Fig. 9 is constructed. The endothermic peaks marked B → A, A → ζ + L and ζ → α + L, obtained on heating, correspond to phase transitions and/or reactions in the sample. The final melting of α could only be detected as a weak, indistinct shoulder on heating, and hence the liquidus temperature (note: subject to supercooling) was extracted from cooling data. The systematic use of TA cooling data is, on the other hand, prevented by the slow equilibrium processes in the solid-state reactions. Reactions which involve two or three phases in the ternary alloys usually proceed over a temperature interval. The width of a peak (represented by the double arrows in Fig. 9 and 10) is used as a measure for the temperature interval of the appropriate reaction in Fig. 9. This is considered as a reasonably good measure when the temperature interval is large compared with the heating rate of 5 °C min^{-1}. The character of the reactions specified in Figs. 9 and 10 is verified by metallography, XPD and high-temperature XPD.

An uncertainty concerning the formation temperatures of the β- and ζ-phases in the Au–Sn system was pointed out in the Introduction. In order to clarify this point, seven samples with compositions in the range $Au_{92}Sn_{08}$–$Au_{80}Sn_{20}$ were examined by DSC at a heating rate of 2 °C min^{-1}. The results (referring to averages of the onset temperatures for endothermic peaks) show that β and ζ form peritectically at

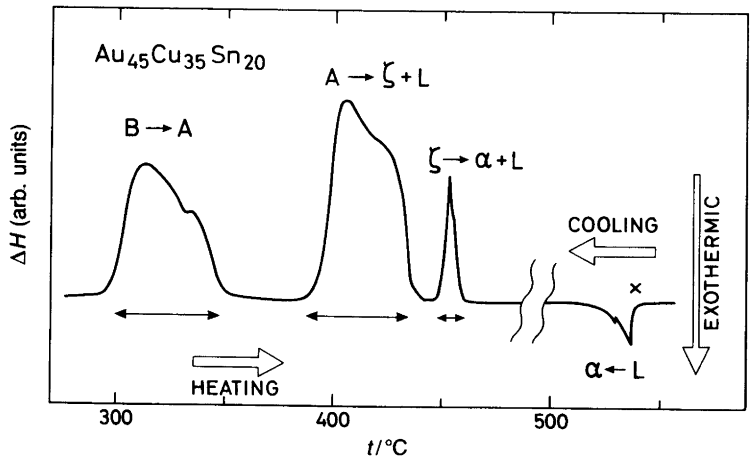

Fig. 10. TA scan of the $Au_{45}Cu_{35}Sn_{20}$ sample fitted on a temperature-independent baseline. Origin in transition or reaction is labelled. The cross and double arrows correspond to symbols used in Fig. 9.

533 ± 1 and 525 ± 1 °C, respectively. These findings thus nicely confirm the results of Legendre *et al.*[7] (incorporated in Fig. 1).

On the substitution of Cu for Au the formation temperature for the β-phase decreases more rapidly than that for the ζ-phase. The phase changes, as these manifest themselves in samples with 20 atom % Sn, are sketched in the inset to Fig. 9. At a certain temperature, indicated as ~515 °C in Fig. 9, there will, assuming constant pressure, exist an invariant four-phase field (α + β + ζ + L). The circumstances around these reactions are, however, not subjected to further examination in this study. At higher Cu contents the β-phase is formed through the reaction α + ζ → β, and β will no longer be represented in Fig. 9, which depicts the situation at 20 atom % Sn.

The reaction ζ → α + L usually proceeds over a temperature interval in the ternary alloys. On an increasing degree of substitution of Cu for Au this conversion passes through a temperature minimum at ~400 °C. At this, so-called indifferent state, the reaction proceeds at constant temperature. The phase situation above this temperature is (somewhat tentatively) illustrated by the isothermal section from the Au–Cu–Sn phase diagram at ~450 °C shown in Fig. 11.

At ~320 °C there exists a four-phase field (α + ζ + δ/η + L), which at 20 atom % Sn extends from 17 to 25 atom % Cu. At constant pressure this must represent an invariant phase field according to the Gibbs phase rule, implying that as

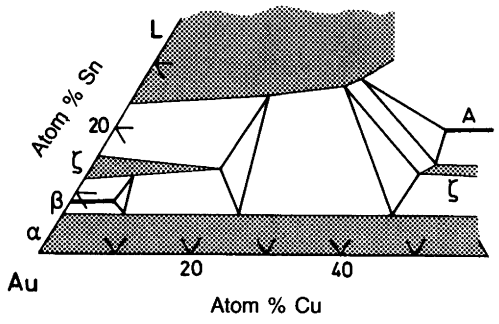

Fig. 11. Tentative isothermal section from Au–Cu–Sn phase diagram at ~450 °C.

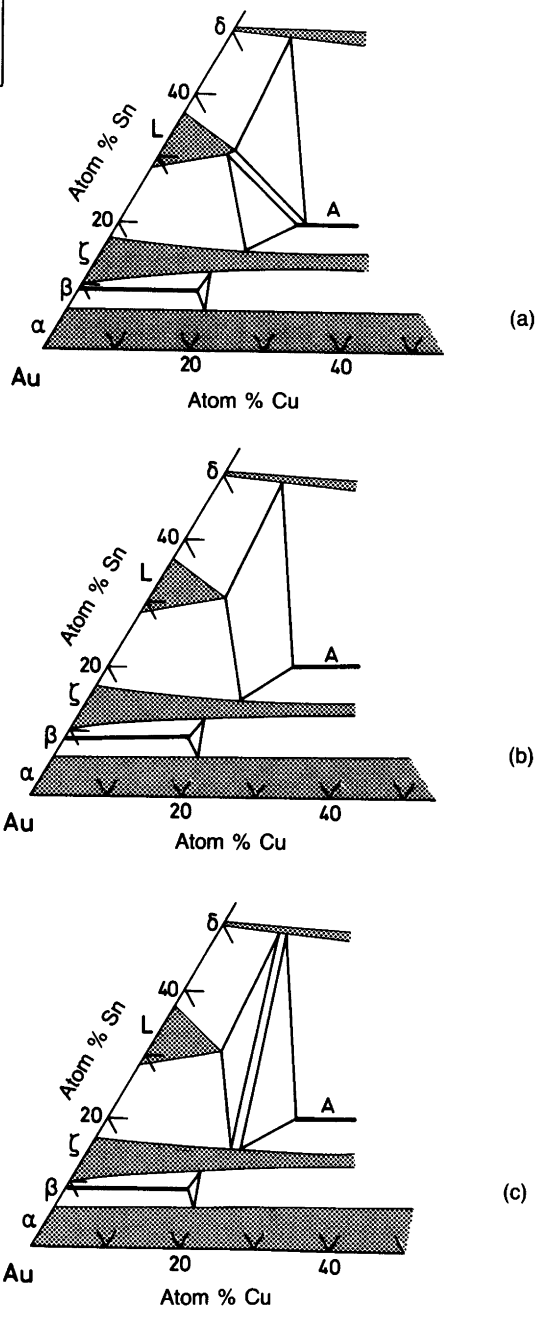

Fig. 12. Isothermal sections from Au–Cu–Sn phase diagram near 320 °C where the invariant state of the ζ + δ/η + A + L four-phase equilibrium occurs (see text): (a) temperature just above the invariant state; (b) situation at the invariant state; (c) temperature just below the invariant state.

long as all the four phases are present neither their composition nor the temperature can be varied. The phase situation at this temperature is depicted in Fig. 12(b), whereas the circumstances at temperatures just above and below the invariant state are illustrated in Figs. 12(a) and (c), respectively. The four-phase field is split by the two-phase field A + L above this temperature [Fig. 12(a)] and by ζ + δ/η below this temperature [Fig. 12(c)]. The conversion thus involved, A + L ⇌ ζ + δ/η, is referred to as a diagonal 2/2 invariant[20] or as a quasi-peritectic[21] reaction.

Concluding considerations

There are always a number of questions which spring to mind when one is faced with a phase diagram like that of Au–Cu–Sn. However, the majority of these cannot be attacked because of a lack of key information. Why the Au–Cu–Sn phase diagram looks like it does, belongs to this category. It is nowadays possible to calculate phase diagrams on the basis of thermodynamic data, and this approach has been used to simulate the binary diagrams of Au–Cu[2] and Au–Sn.[22] The Cu–Sn system has, so far, apparently not been attacked by this technique. An attempt on the ternary Au–Cu–Sn phase diagram has to await the basic thermodynamic data.

The characteristic pointed (extended) shapes of the homogeneity regions in the Au–Cu dimension represents and interesting detail of the Au–Cu–Sn phase diagram (Fig. 8). This is not surprising, since the well established criteria for extensive solid solubility are satisfied. The size difference between Au and Cu, although not negligible, is well within the 15 % criterion of Hume-Rothery.[23] This also shows up in the binary phase diagram for Au–Cu, which exhibits complete solid solubility above 410 °C. Likewise their valences are equal in metallic phases, and the small distinction in electronegativity does certainly not alone remove the compatibility. The problem in this case is rather to account for the differencs in the extensions of the homogeneity regions. In doing so one has to remember that a phase diagram only shows the phases and phase fields that are most stable. This is nicely illustrated for phase A, which probably 'extends' right up to its binary Au–Sn end-point; however, beyond ca. 55 atom % Au, ζ + L or ζ + δ/η (depending on temperature) are more stable (cf. Fig. 9). The fact that there indeed are differences between Au and Cu shows up even in the distinctly different phase diagrams for Au–Sn and Cu–Sn (Figs. 1 and 2).

The detailed discussion of interatomic distances, coordinations and other structural features of the intermediate phases naturally belongs together with the structure determinations which will be reported separately. However, a few brief comments on the gross unit-cell data in terms of atomic volumes may nevertheless be appropriate.

Owing to the pointed shape of the homogeneity regions in the Au–Cu dimension it is possible to estimate the difference between Au and Cu atomic volumes (ΔV_{Au-Cu}) for the solid phases under consideration. ΔV_{Au-Cu} is obtained from the difference in unit-cell volume for two compositions with constant Sn content divided by the difference in the mole fraction $n_{Cu}/(n_{Cu} + n_{Au})$ and by the amount of Au and Cu atoms in the unit cell. The results presented in Fig. 13 show that there is a remarkably systematic increase in ΔV_{Au-Cu} with increasing Sn content. This trend is qualitatively explained on the basis of the electronegativities of the components (Au: 2.3; Cu: 1.8; Sn: 1.8).[23] Starting from the binary α-phase (where ΔV_{Au-Cu} naturally matches the listing of Pearson),[23] introduction of Sn leads to transfer of electron density from Sn to Au without significantly upsetting the balance in the electron distribution between Au and Cu already established at the binary end (a consequence of the equal electronegativity of Cu and Sn). The more Sn atoms that are introduced the more electron density is transferred to the Au atoms. As the result of this process V_{Au} increases with increasing Sn content whereas V_{Cu} will remain virtually constant. Consequently ΔV_{Au-Cu} will increase monotonically with increasing Sn content as found in Fig. 13.

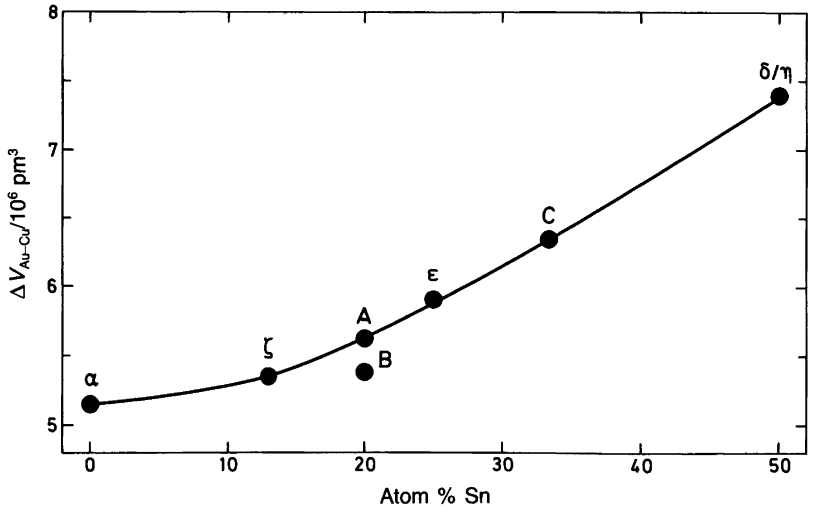

Fig. 13. Atomic volume difference between Au and Cu (ΔV_{Au-Cu}) versus Sn content. For comments concerning phases β and B see text.

It should be noted that the present ΔV_{Au-Cu} value for the β-phase does not fit the trend in Fig. 13. However, this is easily explained as a consequence of the fact that the composition of β is considerably less certain than for the other Au–Cu–Sn phases. Any uncertainty in composition is of course critical, since the slope of the unit-cell volume versus composition plot is used to derive ΔV_{Au-Cu}.

Another important feature is encountered for the B-phase. Here the point marked in Fig. 13 refers to the Cu-rich part of the homogeneity range, whereas the corresponding $\Delta V_{Au-Cu} = 4.43 \times 10^{-6}$ pm^3 for the Au-rich part falls considerably below the trend in the illustration. This apparent defect is accounted for by a variation in the solid solution mechanism within the homogeneity regions. This interesting aspect will be returned to when the structural features of phase B are reported.

References

1. Karlsen, O. B., Kjekshus, A. and Røst, E. *Acta Chem. Scand. 44* (1990) 197.
2. Okamoto, H., Chakrabarti, D. J., Laughlin, D. E., and Massalski, T. B. *Bull. Alloy Phase Diagrams 8* (1987) 454.
3. Sato, H. and Toth, R. S. *Phys. Rev. 124* (1961) 1833.
4. Massalski, T. B. and King, H. W. *Acta Metall. 8* (1960) 667.
5. Schubert, K., Breimer, H. and Gohle, R. *Z. Metallkd. 50* (1959) 146.
6. Okamoto, H. and Massalski, T. B. *Bull. Alloy Phase Diagrams 5* (1984) 492.
7. Legendre, B., Chhay, H. and Prince, A. *Bull. Soc. Chim. Fr.* (1985) I-50.
8. Legendre, B., Chhay, H., Hayes, F., Maxwell, C. A., Evans, D. S. and Prince, A. *Mater. Sci. Technol. 3* (1987) 875.
9. Hansen, M. and Anderko, K. *Constitution of Binary Alloys,* McGraw-Hill, New York 1958.
10. Arnberg, L., Jonsson, A. and Westman, S. *Acta Chem. Scand., Ser. A 30* (1976) 187.
11. Booth, M. H., Brandon, J. K., Brizard, R. Y., Chieh, C. and Pearson, W. B. *Acta Crystallogr., Sect. B 33* (1977) 30.
12. Watanabe, Y., Fujinaga, Y. and Iwasaki, H. *Acta Crystallogr., Sect. B 39* (1983) 306.
13. Roeder, J. F., Notis, M. R. and Goldstein, J. I. *Diffus. Defect Data A 59* (1988) 271.
14. Werner, P. E. *The Computer Program SCANPI,* Institute of Inorganic Chemistry, University of Stockholm, Sweden 1981.
15. Ersson, N. O. *Program CELLKANT,* Chemical Institute, Uppsala University, Uppsala, Sweden 1981.
16. Jan, J.-P., Pearson, W. B., Kjekshus, A. and Woods, S. B. *Can. J. Phys. 41* (1963) 2252.
17. Westgren, A. and Phragmén, G. *Z. Anorg. Chem. 175* (1928) 80.
18. Giessen, B. C. *Z. Metallkd. 59* (1968) 805.
19. Jena, A. K., Giessen, B. C. and Bever, M. B. *Metall. Trans. 4* (1973) 279.
20. Ricchi, J. E. *The Phase Rule and Heterogeneous Equilibrium,* Dover, New York 1966.
21. Prince, A. *Alloy Phase Equilibria,* Elsevier, Amsterdam 1966.
22. Chevalier, P.-Y. *Thermochim. Acta 130* (1988) 1.
23. Pearson, W. B. *The Crystal Chemistry and Physics of Metals and Alloys,* Wiley-Interscience, New York 1972.

Received June 3, 1991.